Published in final edited form as:
Cell Calcium. 2012 July ; 52(1): 93–102. doi:10.1016/j.ceca.2012.04.009.

Calcium-Dependent Physiologic and Pathologic Stimulus-Metabolic Response Coupling in Hepatocytes

Lawrence D. Gaspers, **Elisabeth Mémin**, and **Andrew P. Thomas**
Department of Pharmacology and Physiology University of Medicine and Dentistry of New Jersey 185 South Orange Avenue Newark, NJ 07103

Abstract

A recurrent paradigm in calcium signaling is the coordination of the target response of the calcium signal with activation of metabolic energy production to support that response. This occurs in many tissues, including cardiac and skeletal muscle where contractile activity and ATP production are coordinately regulated by the frequency and amplitude of calcium transients, endocrine and exocrine cells that use calcium to drive the secretory process, and hepatocytes where the downstream targets of calcium include both catabolic and anabolic processes. The primary mechanism by which calcium enhances the capacity for energy production is through calcium-dependent stimulation of mitochondrial oxidative metabolism, achieved by increasing NADH production and respiratory chain flux. Although this enhances energy supply, it also has the potential for deleterious consequences resulting from increased generation of reactive oxygen species (ROS). The negative consequences of calcium-dependent mitochondrial activation can be ameliorated when the underlying cytosolic calcium signals occur as brief calcium spikes or oscillations, with signal strength encoded through the spike frequency (frequency modulation). Frequency modulation increases signal fidelity, and reduces pathological effects of calcium, including excess mitochondrial ROS production and apoptotic or necrotic outcomes. The present article reviews these issues using data obtained in hepatocytes under physiologic and pathologic conditions.

Phosphoinositide-dependent calcium signaling in hepatocytes

The predominant pathway of calcium mobilization in non-excitable cells is mediated by inositol lipid signaling and the intracellular second messenger inositol 1,4,5-trisphosphate ($InsP_3$) [1-3]. In hepatocytes, this signaling pathway plays a key role in regulating processes as diverse as gene expression, bile secretion and the metabolic processing of carbohydrates, amino acids and lipids. In the context of metabolic regulation, $InsP_3$-dependent increases in cytosolic Ca^{2+} ($[Ca^{2+}]_i$) are generally associated with the activation of catabolic metabolism, although one key target, gluconeogenesis, may be looked on as an anabolic pathway of the liver to meet the catabolic demands of other tissues. The primary hormones that act through $InsP_3$ and increases of $[Ca^{2+}]_i$ to regulate hepatic metabolism acutely are epinephrine and norepinephrine, binding to α_1-adrenergic receptors. Other hormones that also activate this pathway include vasopressin, angiotensin II and ATP (acting on $P2_y$ receptors) [4, 5]. Each of these hormones binds to a G-protein-coupled receptor (GPCR) to stimulate phosphoinositide-specific phospholipase C (PLC), predominantly PLC-β and the generation

Correspondence to Dr. Gaspers at the above address Larry.Gaspers@UMDNJ.EDU Phone: 973-972-5379.

of $InsP_3$ and diacylglycerol. In addition to the GPCR-linked hormones, a number of tyrosine kinase receptor-linked hormones, including epidermal growth factor (EGF) and hepatocyte growth factor (HGF) also increase $[Ca^{2+}]_i$ by stimulating PLC-γ to generate $InsP_3$ [4-7]. Interestingly, the HGF receptor (c-Met) appears to translocate to the nucleus to stimulate a localized generation of $InsP_3$, rather than acting on PLC located at the plasma membrane [7].

$InsP_3$ mobilizes Ca^{2+} stored predominantly in the endoplasmic reticulum, but also from other intracellular organelles including the nuclear envelope, by binding to the $InsP_3$ receptor Ca^{2+} channels ($InsP_3R$) [1, 8-10]. In hepatocytes, which make up the bulk of the liver, the major $InsP_3R$ isoforms are Type-1 and Type-2, with the former distributed fairly evenly throughout the cytoplasmic compartment, whereas the latter is localized to the apical membrane of the cell [11, 12]. In addition to activation by $InsP_3$, the $InsP_3Rs$ are sensitive to modulation by $[Ca^{2+}]_i$, with both stimulatory and inhibitory inputs occurring by direct Ca^{2+} interaction with the $InsP_3R$, which can give rise to $[Ca^{2+}]_i$ oscillations [1, 2, 8]. In the liver, these $[Ca^{2+}]_i$ oscillations are highly regular and occur as base-line separated $[Ca^{2+}]_i$ spikes with periods ranging from 0.5 to 10 min [4, 5, 13]. The hepatic $[Ca^{2+}]_i$ oscillations are a particularly good example of frequency modulation, with spike frequency increasing over a wide range as the agonist dose is increased. While it is clear that the positive and negative feedback effects of Ca^{2+} on the $InsP_3Rs$ contribute to the dynamics of the $[Ca^{2+}]_i$ oscillations, it seems likely that an additional feedback of $[Ca^{2+}]_i$ at the level of $InsP_3$ metabolism also plays a role in the low frequency baseline-separated $[Ca^{2+}]_i$ oscillations observed in hepatocytes [14].

Another key feature of hepatic $[Ca^{2+}]_i$ oscillations elicited by hormones and other agonists acting through GPCRs is that they are spatially organized into $[Ca^{2+}]_i$ waves [4, 15]. These $[Ca^{2+}]_i$ waves initiate from a discrete intracellular origin and propagate with fixed velocity and amplitude throughout the cytosol and through the nuclear matrix, apparently through a regenerative process mediated by positive Ca^{2+} feedback. The origin for $[Ca^{2+}]_i$ wave initiation is the same for all agonists in a given cell, and appears to be associated with the concentration of Type-2 $InsP_3Rs$ near to the apical pole of the hepatocyte. Importantly, regenerative $[Ca^{2+}]_i$ wave propagation is not necessarily confined by the boundaries of the cell. In hepatocyte cultures that retain gap junction coupling, and more dramatically in the intact liver, $[Ca^{2+}]_i$ waves initiated in one cell can propagate to neighboring cells, giving rise to intercellular $[Ca^{2+}]_i$ waves. Indeed, in our studies with the intact perfused rat liver, we have shown that hormone-induced $[Ca^{2+}]_i$ waves can travel over long distances crossing entire hepatic lobules encompassing thousands of cell, without loss of amplitude or velocity [4, 16]. These intact tissue experiments have demonstrated that frequency-modulated oscillatory $[Ca^{2+}]_i$ signaling is the predominant mode of physiologic regulation by Ca^{2+}-dependent hormones in liver. As we have reported previously [4, 17, 18], the $[Ca^{2+}]_i$ oscillations in hepatocytes are ideally tuned to regulate mitochondrial metabolism and energy production. In the following sections we discuss coordination of energy production and metabolic regulation under physiological and pathological conditions.

Ca^{2+}-dependent regulation of mitochondrial metabolism

A stimulus-evoked increase in $[Ca^{2+}]_i$ activates contractile, secretory or metabolic pathways and, thus increases utilization of energy stores. The resultant increase in energy demand requires the cell to rapidly increase the rate of ATP production, since even a modest mismatch between consumption and supply will quickly deplete energy reserves leading to tissue dysfunction and most likely the onset of disease states. The maintenance of cellular energy homeostasis requires coordinating the activation of mitochondrial oxidative phosphorylation with the rate of flux through cytosolic ATP-requiring reactions.

Mitochondria are thought to be localized close to Ca^{2+} release sites, such that $[Ca^{2+}]_i$ increases derived from either intracellular stores or influx from the extracellular milieu are rapidly transferred into the mitochondrial matrix to stimulate the Ca^{2+}-sensitive intramitochondrial dehydrogenases and augment the production of mitochondrial NAD(P)H [17-24]. The traces in Fig. 2 show the relationship between Ca^{2+} oscillations and mitochondrial pyridine nucleotide fluorescence over a broad range of stimulus strength. The initial upstroke of the $[Ca^{2+}]_i$ spike is followed closely (2-3 s) by an increase in cellular NAD(P)H fluorescence that predominately originates from the mitochondrial matrix (Fig. 1). Cytosolic Ca^{2+} levels rapidly returned to baseline upon termination of the $[Ca^{2+}]_i$ spike, whereas NAD(P)H oxidation is slower and requires 5-10 minutes to reach basal values (Fig. 2). The relatively slow oxidation phase of NAD(P)H allows mitochondrial redox spikes to fuse together at low rates of Ca^{2+} spiking (≥ 0.5 spikes/min) to produce a sustained level of metabolic output.

Stimulus-induced activation of Ca^{2+}-dependent intramitochondrial dehydrogenases is thought to be one mechanism to coordinate the rate of oxidative phosphorylation with an increase in energy expenditure in the cytosol [19, 24-27]. Indeed, previous studies using adenoviral mediated transduction of adult cardiomyocytes with luciferase to measure cellular ATP levels have shown that cytosolic ATP levels are very stable during the onset of electrical stimulation. In parallel runs, electrical stimulation induced an initial drop in mitochondrial ATP levels followed by a recovery of matrix ATP to values above baseline. The recovery in mitochondrial ATP levels occurred over the same time frame in which there was a stimulus-evoked increase in mitochondrial Ca^{2+} concentration [28]. These results are consistent with a Ca^{2+}-dependent increase in the rate of mitochondrial ATP synthesis during stimulation to supply more ATP and maintain a constant cytosolic phosphorylation potential. More recently, the development of fluorescent ATP-sensitive biosensors (A-TEAM) has allowed direct measurement of cellular ATP levels during hormone stimulation [29-31]. These studies have shown a close correlation between a rise in mitochondrial Ca^{2+} and the increase in mitochondrial matrix ATP levels providing additional evidence supporting the stimulus-metabolic coupling hypothesis [19, 25].

Stimulus-evoked increases in mitochondrial proton motive force

Stimulus-evoked increases in mitochondrial calcium coupled to the activation of intramitochondrial dehydrogenases and electron flux through the respiratory chain is predicted to enhance the magnitude of mitochondrial electrochemical potential [32, 33]. Mitochondrial electrochemical potential or proton motive force (PMF) consists of a mitochondrial membrane potential ($\Delta\Psi_m$) and mitochondrial pH gradient (ΔpH_m). PMF is the driving force for mitochondrial ATP synthesis as well as the transport of substrates (e.g. pyruvate), anions (e.g. phosphate) and cations (e.g. Ca^{2+}) across the mitochondrial inner membrane [34]. Several studies, including our work in primary hepatocytes, have directly measured increases in both components of the electrochemical gradient upon stimulation with hormones or nutrients [17, 24, 35-41]. Moreover, recent studies in INS-1 cells or primary ß-cells indicate that the increases in mitochondrial bioenergetics, particularly increases in mitochondrial pH or ΔpH_m, are critical for prolonged stimulus-induced insulin secretion [39-41]. These studies highlight the importance of this Ca^{2+}-dependent increase in mitochondrial PMF in metabolically active cells.

Stimulus-evoked increases in calcium and mitochondrial PMF can be monitored in real-time by co-loading cells with fura-2/AM and either tetramethyl rhodamine ethyl ester (TMREE), a mitochondrial membrane potential-sensitive dye, or with fluorescein, a weak acid which distributes across the mitochondrial inner membrane according to ΔpH_m [17, 24, 42, 43]. We typically use cells loaded with low levels of TMREE (3-30 nM) for our $\Delta\Psi_m$

measurements to avoid self-quenching of the dye. In this setup, fluorescence intensity of TMREE decreases upon depolarization of the mitochondria. Detailed descriptions of the dye loading protocols and wide-field fluorescence imaging techniques used to carry out these measurements have been published previously [17, 38].

The traces in figure 3 show the simultaneous measurement of vasopressin-evoked increases in $[Ca^{2+}]_i$ and $\Delta\Psi_m$ (Fig. 3A) or the simultaneous measurement of phenylephrine-evoked increases in $[Ca^{2+}]_i$ and ΔpH_m (Fig. 3B-C). The onset of each $[Ca^{2+}]_i$ spike is accompanied by a slow increase in TMREE fluorescence intensity, which we interpret as an increase in the magnitude of $\Delta\Psi_m$. This result is in contrast to the prediction that $\Delta\Psi_m$ might decrease during rapid and electrogenic uptake of Ca^{2+} by the mitochondrial Ca^{2+} uniporter. The hormone-evoked rise in $\Delta\Psi_m$ reached a peak after the $[Ca^{2+}]_i$ spike had already terminated, $\Delta\Psi_m$ then slowly recovered to baseline values. A similar relationship was observed between the frequency of $[Ca^{2+}]_i$ spikes and increases in ΔpH_m. The traces in Fig. 3B show a representative ΔpH_m response to a single agonist-evoked $[Ca^{2+}]_i$ spike. The data indicate that ΔpH_m also increases more slowly than $[Ca^{2+}]_i$, reaching a peak value after the Ca^{2+} spike has returned to baseline. The ΔpH_m was maintained at an elevated plateau for several minutes and then declined gradually. A single Ca^{2+} spike could induce an increase in ΔpH_m that remained above baseline values for 10-15 min beyond the termination of the $[Ca^{2+}]_i$ oscillation. In the example shown in Fig. 3C, the frequency of $[Ca^{2+}]_i$ spiking was sufficient to induce an almost sustained increase in the magnitude of ΔpH_m. An increase in ΔpH_m is expected to occur during active mitochondrial Ca^{2+}-uptake due to proton pumping by the respiratory chain to balance charge movement [34]. However, Ca^{2+}-uptake is relatively brief and essentially complete within seconds, whereas ΔpH_m remains elevated for ten of minutes, indicating that the observed changes in ΔpH_m are not the direct consequence of Ca^{2+}-uptake. As with the increase in NAD(P)H elicited by hormones, stimulus-evoked increases in ΔpH_m and $\Delta\Psi_m$ declined relatively slowly and therefore only followed an oscillatory pattern when the frequency of Ca^{2+} spiking was at or below 0.25 oscillations per min. Thus, discrete oscillations in mitochondrial PMF appear to occur only when there is sufficient time between the $[Ca^{2+}]_i$ spikes to allow Ca^{2+}-dependent increases in NAD(P)H to recover towards baseline values (Fig. 2).

Maximal hormone stimulation also evoked prolonged increases (20-40 min) in mitochondrial PMF despite the fact that mitochondrial Ca^{2+} and NAD(P)H recovered to baseline values at much earlier time points [17, 24]. These data suggest that either 1) Ca^{2+}-dependent activation of a component(s) in the respiratory chain are long lived, 2) hormone stimulation may inhibit pathways dissipating mitochondrial PMF or 3) Ca^{2+}-independent processes, such as the matrix acetyl CoA/CoA ratio or energy charge, may control the respiratory chain activity and mitochondrial PMF during high hormone stimulation. Hormone-evoked increases in $\Delta\Psi_m$ and ΔpH_m occurred even in the presence of oligomycin to block proton flux through the F1-Fo ATP synthetase. These results indicate that the prolonged increase in mitochondrial PMF could not be explained by Ca^{2+}-dependent inhibition of proton flux through the Fo subunit, as observed in some tumor cells [44].

Cellular ROS formation and stimulus-evoked calcium increases

Although stimulus-evoked increases in mitochondrial calcium are essential for activating mitochondrial metabolism, the prolonged elevation of matrix calcium coupled to a sustained increase in mitochondrial PMF are predicted to favor the formation of mitochondrial reactive oxygen species (ROS), superoxide anion ($O_2^{\cdot -}$) and H_2O_2 [45, 46]. The relationship between the rates of mitochondrial ROS production and the magnitude of $\Delta\Psi_m$ is most clearly observed in isolated mitochondrial preparations in the presence of saturating concentrations succinate, i.e. conditions that favor reverse electron flow through NADH

dehydrogenase [46-51]. In these studies, production of H_2O_2 was inhibited by physiological (e.g. ADP) or pharmacological (e.g. uncouplers) maneuvers which lowered $\Delta\Psi_m$. It should be pointed out that the magnitude of substrate-supported ROS formation is highly dependent on the experimental conditions, which are often outside the physiological range. Thus, the often quoted estimate of 1-2% of the total oxygen consumed being converted to $O_2^{\cdot-}$ is only applicable to isolated mitochondria under defined conditions. Presumably, the rates of mitochondrial ROS formation in intact cells are a fraction of these *in vitro* estimates [46, 52]. While the mitochondria are undoubtedly a major source of ROS *in vivo*, the absolute rates of mitochondrial $O_2^{\cdot-}$ and H_2O_2 are difficult to measure as well as the relationship between stimulus-evoked Ca^{2+} increases and mitochondrial ROS formation.

We employed genetically encoded biosensors sensitive to changes in superoxide anion [53] or hydrogen peroxide [54] concentrations to examine whether hormone-evoked increases in Ca^{2+} also stimulate the rates of mitochondrial ROS production in primary cultured hepatocytes. It has been previously shown that increasing levels of $O_2^{\bullet-}$ enhance the fluorescence intensity of circularly permeated yellow fluorescence protein (cpYFP) at 485nm excitation, while the intensity at 410nm remains constant [53]. Insertion of the cpYFP moiety into the regulatory domain of the *E. coli* OxyR protein produces a probe sensitive to submicromolar H_2O_2 concentrations that no longer responds to $O_2^{\bullet-}$ levels [54]. This biosensor, termed Hyper, displays opposite and fully reversible changes at 485nm and 410nm excitation upon H_2O_2 addition; the peroxide increases the 485nm fluorescence intensity while proportionally decreasing the 410nm signal. Thus, the cellular levels of either $O_2^{\bullet-}$ or H_2O_2 can be monitored independent of protein expression by following the F485/F410 ratio over time. These ratiometric techniques are similar to those developed for Ca^{2+}-sensitive probes, such as the Cameleon family.

Hepatocytes isolated from chow-fed animals were transiently transfected using Nucleofection technology (Lonza) then cultured overnight to allow expression of the biosensors. The confocal image stack shown in Fig. 4A indicates that the ROS-sensitive fluorescent proteins are correctly targeted to the mitochondria in primary hepatocytes. Hepatocytes expressing mitochondrial-targeted cpYFP were co-loaded with fura-2/AM to simultaneously monitor $[Ca^{2+}]_i$ and the production of mitochondrial $O_2^{\bullet-}$. Fura-2 and cpYFP fluorescence images were acquired by sequential excitation at 340 ± 10, 380 ± 10 and 485 ± 25 nm. Emitted fluorescence was collected with a 515 nm long band pass dichroic mirror and a 520 nm long band pass filter, as described in [38]. Since the fura-2 absorption spectrum overlaps with cpYFP and predominates at 410nm, the fluorescence intensity of cpYFP can only be monitored at 485nm in these experiments. The data show that treating hepatocytes with 100 nM vasopressin evokes a sustained increase in $[Ca^{2+}]_i$ and after a short delay a slow rise in mitochondrial $O_2^{\cdot-}$ levels, which remained above baseline values over the time-course of the experiment. Similar results were obtained in hepatocytes expressing mitochondrial-targeted Hyper and challenged with ATP concentrations that routinely evoke sustained increases in $[Ca^{2+}]_i$. Hepatocytes express both G-protein coupled P2Y receptors [55] and ligand-gated P2X channels [56] and, thus ATP stimulation is expected to mobilize internal Ca^{2+} stores and stimulate Ca^{2+} influx from the extracellular milieu. The results show that stimulation with ATP induces a dose-dependent increase in emission ratio of mitochondrial-targeted Hyper (Fig. 4C). The addition of excess BAPTA free acid to chelate extracellular Ca^{2+} resulted in a decrease in ATP-stimulated mitochondrial H_2O_2 formation (Fig. 4D). The decline in the Hyper emission ratio after BAPTA treatment occurred after a short delay suggesting that a decrease in intracellular Ca^{2+} precedes or parallels the change in mitochondrial ROS production. Simultaneous fura-2 and mitochondrial ROS measurements could not be carried out under the Ca^{2+}-free condition, because maximal ATP stimulation alters hepatocyte morphology in the absence of extracellular calcium and thus precludes single wavelength measurements like those in Fig. 4B. In parallel experiments, we

transfected hepatocytes with Hyper targeted to the cytosol. Here, ATP stimulation in the presence of extracellular Ca^{2+} did not increase the emission ratio, suggesting that the H_2O_2 increases elicited by Ca^{2+}-dependent hormones are largely confined to the mitochondrial matrix (not shown).

Agonist -evoked increases in the apparent rate of mitochondrial H_2O_2 production were predominantly observed in cells stimulated with maximal hormone concentrations as typified in Fig. 4B-D. A similar increase in H_2O_2 production was observed when hepatocytes were treated with thapsigargin (not shown) to induce sustained increases in both cytosolic and mitochondrial Ca^{2+} [18, 24]. By contrast, challenging the cultures with submaximal hormone doses that induce baseline-separated $[Ca^{2+}]_i$ spiking had little to no effect on the rates of mitochondrial ROS formation. Moreover, when hepatocytes were exposed to low concentrations of ionomycin (100 nM), which induced a small 100-150 nM $[Ca^{2+}]_i$ rise, there was also no effect on the emission ratio of mitochondrial-targeted Hyper (not shown). Taken together, these data suggest that prolonged stimulation with maximal hormone concentrations and/or high levels of intracellular Ca^{2+} promote the formation of mitochondrial oxidants, whereas Ca^{2+} oscillations or small increases in $[Ca^{2+}]_i$ are ineffective stimuli. Thus, protection against Ca^{2+}-induced oxidative stress can be considered as another example of the advantages of frequency-modulated $[Ca^{2+}]_i$ oscillations over sustained $[Ca^{2+}]_i$ signals.

A potential limitation of all protein-based biosensors, particularly cpYFP, is the potential for artifacts due to changes in cellular pH [57]. Physiologically relevant changes in pH can affect the emission ratio independent of oxidant levels: acidification decreases and alkalinization increases the emission ratio of both cpYFP and Hyper. Thus, one could argue that the observed increases in cpYFP and Hyper fluorescence intensities could be due the hormone-evoked rises in mitochondrial pH. However, pH-dependent effects on the biosensors cannot fully explain our results. First, treating cells with ionomycin is expected to increase mitochondrial calcium and decrease matrix pH, yet this challenge failed to decrease the fluorescence intensity of Hyper as would be expected for maneuvers that acidify the mitochondria [37]. Second, maximal hormone stimulation consistently increased the production of mitochondrial oxidants, whereas submaximal hormone doses had little effect on mitochondrial ROS, even though both stimulation protocols evoke rises in mitochondrial pH (Fig. 4 and [17]).

We further explored the relationship between magnitude of mitochondrial ROS production and the magnitude of mitochondrial PFM by treating hepatocytes with protonophores and respiratory inhibitors. The traces in Fig 5A show that the addition of a weak protonophore, 2,4 dinitrophenol (DNP), to partially depolarize the mitochondrial $\Delta\Psi_m$, induces a small drop in the Hyper emission ratio in the mitochondria. Thus far, we have not been able detect a change in mitochondrial PMF (see [58]) with these low concentrations of DNP indicating that Hyper is reporting a true decrease in mitochondrial ROS production rather than responding to a drop in matrix pH. The subsequent addition of CCCP plus oligomycin to completely collapse mitochondrial PMF resulted in a further decrease in the Hyper emission ratio, but this treatment is expected to strongly acidify the mitochondrial matrix, making these results more difficult to interpret solely as changes in mitochondrial ROS. The addition of antimycin A, rotenone (Fig. 5B) and/or myxothiazol (not shown) all induced a slow decrease in the emission ratio of mitochondrially-targeted Hyper. These data are consistent with the idea that the rate of mitochondrial ROS production slows down when there is a drop in mitochondrial PMF. The Hyper emission ratio remained lower than baseline values for 5-20 min then slowly started to increase over time. This slow recover was followed by a rapid and large amplitude increase in the emission ratio of mitochondrial-targeted Hyper for both CCCP and respiratory inhibitors (Figs. 5A, 5B). The subsequent

addition of exogenous H_2O_2 (100 to 300 μM) did not further increase the emission ratio indicating that the probe was fully oxidized after the ROS burst. The onset of the ROS burst was highly variable between cells within the same field of view and occurred anywhere between 15 to 90 min after the addition of the mitochondrial toxins.

Hyper targeted to the cytosol also displayed a biphasic response to mitochondrial respiratory inhibitors. The data in Fig. 5C indicate that inhibiting Complex 1 with rotenone causes an initial decrease in emission ratio of cytosolic Hyper that closely paralleled the drop in mitochondrial Hyper signal. After a short delay (5-10 min), the emission ratio started to recover and eventually rose above baseline values. The large amplitude ROS burst observed in the mitochondrial matrix after prolonged incubation with mitochondrial toxins was not observed over the time-course of this experiment (Fig. 5C), but was observed in other studies just prior to disruption of the plasma membrane (not shown).

Taken together, we interpret the data in Fig. 5 to indicate that dissipating of $\Delta\Psi_m$ initially lowers the production of mitochondrial ROS which, in turn, decreases the rate of mitochondrial H_2O_2 entering the cytosol and, thus the amount of oxidants detected by cytosolic Hyper. In the presence of protonophores or respiratory inhibitors, reducing equivalents required for regenerating mitochondrial GSH or thioredoxin are eventually depleted resulting in a large and rapid increase in mitochondrial and cytosolic ROS levels, as observed in Figs. 5A, 5B. Thus, the dual actions of stimulated mitochondrial metabolism to generate ROS through mitochondrial respiratory chain activity and provide the reducing equivalents for their elimination through increased dehydrogenase activity, can explain why respiratory chain inhibitors, uncouplers and oligomycin can all cause a large increase in ROS production, despite opposite effects on electron flow and the PMF.

Balancing the need for an increase in ATP supply with the generation of potentially toxic radicals is undoubtedly a difficult mission to achieve. Reactive oxygen species have long been implicated in disease processes, but recent studies have suggested that low levels of H_2O_2 may also play a critical role in cell signaling [52, 59-62]. A transient increase in cellular H_2O_2 production is a normal part of the signal transduction cascade evoked by growth factor and cytokine stimulation and is essential for dictating the eventual biological outcome [60, 63-65]. ROS-dependent signals are proposed to convey information by mediating the reversible sulfenation [61] or the formation of a sulphenyl-amide intermediates [66] with redox-sensitive cysteine residues resulting in a change of enzymatic activity. The first described and best characterized classes of proteins sensitive to oxidative modification are phosphatases including protein tyrosine phosphatase 1b [67, 68], phosphatase and tensin homolog (PTEN) and MAPK phosphatases [60]. Stimulus-evoked increases in H_2O_2 levels are proposed to oxidize and inhibit protein tyrosine phosphatases allowing prolonged activation of MAP kinase signaling [52, 60]. Future work is needed to delineate whether Ca^{2+}-dependent increases in mitochondrial H_2O_2 acts as a signaling molecule in this type of cascade, or are the toxic consequences of living in an aerobic world.

Lipid droplets and mitochondria

Chronic alcohol consumption or excessive intake of nutrients are major causes of fatty liver disease and have become global public health problems [69-72] with costs estimated at nearly $2 billion a year in 2000 for the US alone [73]. Long-term and excessive alcohol abuse can lead to a spectrum of liver diseases ranging from alcoholic fatty liver (steatosis), alcoholic steatohepatitis and cirrhosis [69]. Nonalcoholic fatty liver disease (NAFLD) and it more serious variant nonalcoholic steatohepatitis (NASH) are another variety of liver diseases associated with metabolic disorders, such as type2 diabetes and obesity. The

pervasiveness of NAFLD in the general population is on the rise; paralleling the rise in obesity [74].

Alcoholic steatohepatitis and NASH present with similar clinical attributes suggesting a possible common mechanism underlying the development if these pathologies [75]. The earliest common symptom of excessive alcohol or lipid intake is the marked deposition of triglycerides in organelles called lipid droplets. Fat accumulation or steatosis is considered the “first hit” in the progression to more serious forms of liver disease by predisposing hepatocytes to injury induced by “secondary insults” including oxidative stress [76, 77] and pro-inflammatory cytokines, such as TNFα [78]. Although the formation and accumulation of lipid droplets is a common feature for both alcoholic and nonalcoholic liver diseases, the molecular mechanisms regulating the biogenesis and expansion of lipid droplets in the presence of surplus energy supplies or the lipolysis of stored triglycerides during starvation have not been fully delineated in hepatocytes [79].

Surplus intracellular fats are stored in organelles called lipid droplets (LD), which are composed of a single phospholipid monolayer surrounding a neutral lipid core. Lipid droplets are thought to bud off of the endoplasmic reticulum (ER) and remain either attached to the ER or in very close association with it [80-82]. Lipid droplets have been shown to interact with other organelles, including the mitochondria, early endosomes, peroxisomes, as well as with the plasma membrane; presumably trafficked to their final destination by the plethora of Rab GTPases found on the surface of LD [83]. The logical functional link between mitochondria or peroxisomes with LD would be a ready supply of fatty acids derived from lipolysis for the production of ATP in the ß-oxidation pathway. Indeed, the LD-scaffolding protein, perilipin 5, has been implicated in tethering mitochondria to LD in neonatal cardiomyocytes and regulating the local rates of lipolysis and, thus fatty acid flux into the mitochondria [84]. These studies suggested a close physical and functional interaction between the ER, LD and the mitochondria. Our preliminary data suggest that these close associations also suggest the potential for local Ca^{2+} signaling in the regulation of LD metabolism.

Previously electron microscopy studies have described the close interaction between the LD and ER as an egg (LD) inside an egg holder (ER) [85]. These results suggest that ER resident proteins involved in calcium signaling could also localize with LD. To test this idea, we carried out immunofluorescence studies to determine the subcellular distribution of calreticulin, a major ER Ca^{2+}-binding protein, and the SR/ER Ca^{2+}-ATPase (SERCA). In these studies, rats were fed the Lieber-DeCarli alcohol-containing liquid diet to induce fatty liver disease, while littermates controls received an isocaloric diet with carbohydrate substituted for ethanol [86]. Alcoholic hepatocytes were loaded with a red fluorescent fatty acid analogue (10 μM, Bodipy® 558/568 C_{12}) in the presence of 1% (w/v) fatty acid-free bovine serum albumin (BSA) for 2 hrs prior to fixation with 1% paraformaldehyde. The fluorescence of Bodipy® 558/568 C_{12} allows the visualization of LD distribution and morphology, while secondary immunofluorescence can be detected with an Alexa 488-conjugated secondary antibody without significant spectral overlap between the fluorophores. In parallel studies, hepatocytes isolated from animals fed a control diet were co-loaded with Bodipy® 558/568 C_{12} plus 300 μM oleic acid bound to BSA to induce LD formation independent of alcohol consumption. The confocal images in Fig 6 indicate that both calreticulin (top row, green pseudocolor) and SERCA (middle row, green pseudocolor) immunoreactivity form ring-like structures around LD (red pseudocolor). This co-localization occurred in hepatocytes isolated from alcohol-fed rats or in control liver cells treated with oleic acid to induce the formation of LD (Fig. 6, top and middle rows, respectively). The intricate mesh-like structure of the ER was better visualized in live hepatocytes stained with ER tracker compared to fixed cells (Fig. 6 bottom left panels). In

these studies, hepatocytes from chow-fed rats were co-stained with ER tracker and Bodipy® 558/568 C_{12}. Confocal images of the fluorophores were acquired by sequentially exciting the sample with a multiphoton laser tuned to 720nm and then with a 543nm HeNe laser. These images show an extensive network of ER tubules surrounding and enveloping each LD and in some cases the tubular ER structures infiltrating clusters of LD. We have also carried out immunofluorescence studies to determine the localization of inositol 1,4,5-trisphosphate ($InsP_3$) receptors in lipid-loaded hepatocytes. Hepatocytes express both type 1 and type 2 $InsP_3$ receptors; the type 2 $InsP_3$ receptor is the predominate isoform and is concentrated in a domain close to the bile canalicular membrane, while type 1 $InsP_3$ receptors are expressed diffusely throughout the cytoplasm [12]. The data indicate that the formation and accumulation of large LD does not dramatically alter the distribution of either type 1 or type 2 $InsP_3$ receptors (not shown). Presumably, $InsP_3$ receptors are still present in the ER membrane surrounding the LD, just not concentrated enough to be detected by immunofluorescence techniques.

Live cell imaging also revealed the close association between LD and mitochondria in primary cultured hepatocytes. The location of LD and mitochondria was determined by acquiring confocal images of hepatocytes transiently expressing a mitochondrially-targeted glutathione biosensor Grx1-roGFP2 (Fig. 6, rightmost panel on bottom row) or a mitochondrially-targeted Ca^{2+}-sensitive fluorescent protein, together with the Bodipy® 558/568 C_{12} staining (Fig. 7). The confocal images indicate that subsets of mitochondria are in close proximity with each LD. Mitochondria in primary hepatocytes do not undergo significant movement as compared to mitochondria in other cells types or in hepatoma cell lines. Thus, the same set of mitochondria remained in juxtaposition with the LD for extended periods of time and few mitochondria were observed to traffic to or from the LD over the time course of the experiments (30-60 min).

For the experiments of Fig. 7, hepatocytes isolated from chow-fed rats were transfected with mitochondrial-targeted GcamP3, and then cultured overnight with oleic acid and Bodipy® 558/568 C_{12} to induce the formation and accumulation of LD. Fatty acids were removed 2-4 hrs prior to experimentation to favor the hydrolysis of stored triglycerides. The data using GcamP3 show spontaneous and transient increases in mitochondrial matrix calcium levels under basal conditions, predominately in mitochondrion associated with the LD (Fig. 7). Spontaneous increases in mitochondrial Ca^{2+} levels were not readily observed in the absence of lipid loading, suggesting the formation of a local Ca^{2+} signaling network during the formation of the LD. In this proposed scheme, Ca^{2+} released from the ER surrounding LD would be rapidly accumulated by mitochondria tethered to LD to locally stimulate mitochondrial metabolism and the oxidation of fatty acids [19]. The nature of the Ca^{2+}-mobilizing signal or the ER Ca^{2+}-release channels are currently unknown. We predict that these local Ca^{2+} signals are required for efficient oxidation of fatty acids derived from LD. Moreover, defining the molecules involved in the local Ca^{2+} signaling pathway may provide additional targets for therapeutic intervention of fatty liver diseases.

Acknowledgments

This work was supported by NIH grants AA017752 to LDG and DK82954 & DK078019 to APT. Dr. Thomas is also supported by the Thomas P. Infusion Endowed Chair.

REFERENCES

1. Berridge MJ. Inositol trisphosphate and calcium signalling. Nature. 1993; 361:315–325. [PubMed: 8381210]
2. Clapham DE. Calcium signaling. Cell. 1995; 80:259–268. [PubMed: 7834745]

3. Rhee SG. Regulation of phosphoinositide-specific phospholipase C. Annu Rev Biochem. 2001; 70:281–312. [PubMed: 11395409]
4. Gaspers LD, Thomas AP. Calcium signaling in liver. Cell Calcium. 2005; 38:329–342. [PubMed: 16139354]
5. Gaspers, LD.; Pierobon, N.; Thomas, AP. Calcium signaling. In: Dufour, JF.; Clavien, P-A., editors. Signaling Pathways in Liver Disease. Springer-Verlag GmbH & Co. KG; Heidelberg, Germany: 2005. p. 211-221.
6. Nathanson MH, Schlosser SF. Calcium signaling mechanisms in liver in health and disease. Prog Liver Dis. 1996; 14:1–27. [PubMed: 9055572]
7. Gomes DA, Rodrigues MA, Leite MF, Gomez MV, Varnai P, Balla T, Bennett AM, Nathanson MH. c-Met must translocate to the nucleus to initiate calcium signals. J Biol Chem. 2008; 283:4344–4351. [PubMed: 18073207]
8. Patel S, Joseph SK, Thomas AP. Molecular properties of inositol 1,4,5-trisphosphate receptors. Cell Calcium. 1999; 25:247–264. [PubMed: 10378086]
9. Gomes DA, Leite MF, Bennett AM, Nathanson MH. Calcium signaling in the nucleus. Can J Physiol Pharmacol. 2006; 84:325–332. [PubMed: 16902580]
10. Gerasimenko J, Maruyama Y, Tepikin A, Petersen OH, Gerasimenko O. Calcium signalling in and around the nuclear envelope. Biochem Soc Trans. 2003; 31:76–78. [PubMed: 12546657]
11. Hernandez E, Leite MF, Guerra MT, Kruglov EA, Bruna-Romero O, Rodrigues MA, Gomes DA, Giordano FJ, Dranoff JA, Nathanson MH. The spatial distribution of inositol 1,4,5-trisphosphate receptor isoforms shapes Ca2+ waves. J Biol Chem. 2007; 282:10057–10067. [PubMed: 17284437]
12. Hirata K, Pusl T, O'Neill AF, Dranoff JA, Nathanson MH. The type II inositol 1,4,5-trisphosphate receptor can trigger Ca2+ waves in rat hepatocytes. Gastroenterology. 2002; 122:1088–1100. [PubMed: 11910359]
13. Rooney TA, Sass EJ, Thomas AP. Characterization of cytosolic calcium oscillations induced by phenylephrine and vasopressin in single fura-2-loaded hepatocytes. J Biol Chem. 1989; 264:17131–17141. [PubMed: 2793847]
14. Politi A, Gaspers LD, Thomas AP, Hofer T. Models of IP3 and Ca2+ oscillations: frequency encoding and identification of underlying feedbacks. Biophys J. 2006; 90:3120–3133. [PubMed: 16500959]
15. Rooney TA, Renard DC, Sass EJ, Thomas AP. Oscillatory cytosolic calcium waves independent of stimulated inositol 1,4,5-trisphosphate formation in hepatocytes. J Biol Chem. 1991; 266:12272–12282. [PubMed: 2061312]
16. Robb-Gaspers LD, Thomas AP. Coordination of Ca2+ signaling by intercellular propagation of Ca2+ waves in the intact liver. J Biol Chem. 1995; 270:8102–8107. [PubMed: 7713913]
17. Robb-Gaspers LD, Burnett P, Rutter GA, Denton RM, Rizzuto R, Thomas AP. Integrating cytosolic calcium signals into mitochondrial metabolic responses. Embo J. 1998; 17:4987–5000. [PubMed: 9724635]
18. Hajnóczky G, Robb-Gaspers LD, Seitz MB, Thomas AP. Decoding of cytosolic calcium oscillations in the mitochondria. Cell. 1995; 82:415–424. [PubMed: 7634331]
19. McCormack JG, Halestrap AP, Denton RM. Role of calcium ions in regulation of mammalian intramitochondrial metabolism. Physiol Rev. 1990; 70:391–425. [PubMed: 2157230]
20. Pralong WF, Hunyady L, Varnai P, Wollheim CB, Spat A. Pyridine nucleotide redox state parallels production of aldosterone in potassium-stimulated adrenal glomerulosa cells. Proc Natl Acad Sci U S A. 1992; 89:132–136. [PubMed: 1729679]
21. Rizzuto R, Brini M, Murgia M, Pozzan T. Microdomains with high Ca2+ close to IP3-sensitive channels that are sensed by neighboring mitochondria. Science. 1993; 262:744–747. [PubMed: 8235595]
22. Lawrie AM, Rizzuto R, Pozzan T, Simpson AW. A role for calcium influx in the regulation of mitochondrial calcium in endothelial cells. J Biol Chem. 1996; 271:10753–10759. [PubMed: 8631885]
23. Pralong WF, Spat A, Wollheim CB. Dynamic pacing of cell metabolism by intracellular Ca2+ transients. J Biol Chem. 1994; 269:27310–27314. [PubMed: 7961642]

24. Robb-Gaspers LD, Rutter GA, Burnett P, Hajnoczky G, Denton RM, Thomas AP. Coupling between cytosolic and mitochondrial calcium oscillations: role in the regulation of hepatic metabolism. Biochim Biophys Acta. 1998; 1366:17–32. [PubMed: 9714714]
25. Denton RM. Regulation of mitochondrial dehydrogenases by calcium ions. Biochim Biophys Acta. 2009; 1787:1309–1316. [PubMed: 19413950]
26. Voronina SG, Barrow SL, Simpson AW, Gerasimenko OV, da Silva Xavier G, Rutter GA, Petersen OH, Tepikin AV. Dynamic changes in cytosolic and mitochondrial ATP levels in pancreatic acinar cells. Gastroenterology. 2010; 138:1976–1987. [PubMed: 20102715]
27. Cardenas C, Miller RA, Smith I, Bui T, Molgo J, Muller M, Vais H, Cheung KH, Yang J, Parker I, Thompson CB, Birnbaum MJ, Hallows KR, Foskett JK. Essential regulation of cell bioenergetics by constitutive InsP3 receptor Ca2+ transfer to mitochondria. Cell. 2010; 142:270–283. [PubMed: 20655468]
28. Bell CJ, Bright NA, Rutter GA, Griffiths EJ. ATP regulation in adult rat cardiomyocytes: time-resolved decoding of rapid mitochondrial calcium spiking imaged with targeted photoproteins. J Biol Chem. 2006; 281:28058–28067. [PubMed: 16882672]
29. Zhao Y, Araki S, Wu J, Teramoto T, Chang YF, Nakano M, Abdelfattah AS, Fujiwara M, Ishihara T, Nagai T, Campbell RE. An expanded palette of genetically encoded Ca(2) indicators. Science. 2011; 333:1888–1891. [PubMed: 21903779]
30. Imamura H, Nhat KP, Togawa H, Saito K, Iino R, Kato-Yamada Y, Nagai T, Noji H. Visualization of ATP levels inside single living cells with fluorescence resonance energy transfer-based genetically encoded indicators. Proc Natl Acad Sci U S A. 2009; 106:15651–15656. [PubMed: 19720993]
31. Nakano M, Imamura H, Nagai T, Noji H. Ca(2) regulation of mitochondrial ATP synthesis visualized at the single cell level. ACS Chem Biol. 2011; 6:709–715. [PubMed: 21488691]
32. Koretsky AP, Balaban RS. Changes in pyridine nucleotide levels alter oxygen consumption and extra-mitochondrial phosphates in isolated mitochondria: a 31P-NMR and NAD(P)H fluorescence study. Biochim Biophys Acta. 1987; 893:398–408. [PubMed: 2888484]
33. Brown GC, Lakin-Thomas PL, Brand MD. Control of respiration and oxidative phosphorylation in isolated rat liver cells. Eur J Biochem. 1990; 192:355–362. [PubMed: 2209591]
34. Nicholls, DG. Bioenergetics: An introduction to the Chemiosmotic Theory. First ed.. Academic Press Inc.; New York, New York: 1982.
35. Jouaville LS, Pinton P, Bastianutto C, Rutter GA, Rizzuto R. Regulation of mitochondrial ATP synthesis by calcium: evidence for a long-term metabolic priming. Proc Natl Acad Sci U S A. 1999; 96:13807–13812. [PubMed: 10570154]
36. Maechler P, Wollheim CB. Mitochondrial glutamate acts as a messenger in glucose-induced insulin exocytosis. Nature. 1999; 402:685–689. [PubMed: 10604477]
37. Abad MF, Di Benedetto G, Magalhaes PJ, Filippin L, Pozzan T. Mitochondrial pH monitored by a new engineered green fluorescent protein mutant. J Biol Chem. 2004; 279:11521–11529. [PubMed: 14701849]
38. Gaspers LD, Thomas AP. Calcium-dependent activation of mitochondrial metabolism in mammalian cells. Methods. 2008; 46:224–232. [PubMed: 18854213]
39. Wiederkehr A, Wollheim CB. Mitochondrial signals drive insulin secretion in the pancreatic beta-cell. Mol Cell Endocrinol. 2011
40. Akhmedov D, Braun M, Mataki C, Park KS, Pozzan T, Schoonjans K, Rorsman P, Wollheim CB, Wiederkehr A. Mitochondrial matrix pH controls oxidative phosphorylation and metabolism-secretion coupling in INS-1E clonal beta cells. FASEB J. 2010; 24:4613–4626. [PubMed: 20647546]
41. Wiederkehr A, Park KS, Dupont O, Demaurex N, Pozzan T, Cline GW, Wollheim CB. Matrix alkalinization: a novel mitochondrial signal for sustained pancreatic beta-cell activation. EMBO J. 2009; 28:417–428. [PubMed: 19165153]
42. Thomas PJ, Gaspers LD, Pharr C, Thomas JA. Continuous measurement of mitochondrial pH gradients in isolated hepatocytes by difference ratio spectroscopy. Arch Biochem Biophys. 1991; 288:250–260. [PubMed: 1898020]

43. Loew LM, Tuft RA, Carrington W, Fay FS. Imaging in five dimensions: time-dependent membrane potentials in individual mitochondria. Biophys J. 1993; 65:2396–2407. [PubMed: 8312478]
44. Bogucka K, Teplova VV, Wojtczak L, Evtodienko YV, Wojtczaka L. Inhibition by Ca2+ of the hydrolysis and the synthesis of ATP in Ehrlich ascites tumour mitochondria: relation to the Crabtree effect. Biochim Biophys Acta. 1995; 1228:261–266. [PubMed: 7893730]
45. Brookes PS, Yoon Y, Robotham JL, Anders MW, Sheu SS. Calcium, ATP, and ROS: a mitochondrial love-hate triangle. Am J Physiol Cell Physiol. 2004; 287:C817–833. [PubMed: 15355853]
46. Murphy MP. How mitochondria produce reactive oxygen species. Biochem J. 2009; 417:1–13. [PubMed: 19061483]
47. Boveris A, Chance B. The mitochondrial generation of hydrogen peroxide. General properties and effect of hyperbaric oxygen. Biochem J. 1973; 134:707–716. [PubMed: 4749271]
48. Chance B, Sies H, Boveris A. Hydroperoxide metabolism in mammalian organs. Physiol Rev. 1979; 59:527–605. [PubMed: 37532]
49. Hansford RG, Hogue BA, Mildaziene V. Dependence of H2O2 formation by rat heart mitochondria on substrate availability and donor age. J Bioenerg Biomembr. 1997; 29:89–95. [PubMed: 9067806]
50. Korshunov SS, Skulachev VP, Starkov AA. High protonic potential actuates a mechanism of production of reactive oxygen species in mitochondria. FEBS Lett. 1997; 416:15–18. [PubMed: 9369223]
51. Andreyev AY, Kushnareva YE, Starkov AA. Mitochondrial metabolism of reactive oxygen species. Biochemistry (Mosc). 2005; 70:200–214. [PubMed: 15807660]
52. Finkel T. Signal transduction by mitochondrial oxidants. J Biol Chem. 2012; 287:4434–4440. [PubMed: 21832045]
53. Wang W, Fang H, Groom L, Cheng A, Zhang W, Liu J, Wang X, Li K, Han P, Zheng M, Yin J, Wang W, Mattson MP, Kao JP, Lakatta EG, Sheu SS, Ouyang K, Chen J, Dirksen RT, Cheng H. Superoxide flashes in single mitochondria. Cell. 2008; 134:279–290. [PubMed: 18662543]
54. Belousov VV, Fradkov AF, Lukyanov KA, Staroverov DB, Shakhbazov KS, Terskikh AV, Lukyanov S. Genetically encoded fluorescent indicator for intracellular hydrogen peroxide. Nat Methods. 2006; 3:281–286. [PubMed: 16554833]
55. Dixon CJ, Woods NM, Webb TE, Green AK. Evidence that rat hepatocytes co-express functional P2Y1 and P2Y2 receptors. Br J Pharmacol. 2000; 129:764–770. [PubMed: 10683201]
56. Gonzales E, Prigent S, Abou-Lovergne A, Boucherie S, Tordjmann T, Jacquemin E, Combettes L. Rat hepatocytes express functional P2X receptors. FEBS Lett. 2007; 581:3260–3266. [PubMed: 17597621]
57. Roma LP, Duprez J, Takahashi HK, Gilon P, Wiederkehr A, Jonas JC. Dynamic measurements of mitochondrial hydrogen peroxide concentration and glutathione redox state in rat pancreatic beta-cells using ratiometric fluorescent proteins: confounding effects of pH with HyPer but not roGFP1. Biochem J. 2012; 441:971–978. [PubMed: 22050124]
58. Turner JD, Gaspers LD, Wang G, Thomas AP. Uncoupling protein-2 modulates myocardial excitation-contraction coupling. Circ Res. 2010; 106:730–738. [PubMed: 20056920]
59. Chandel NS, Maltepe E, Goldwasser E, Mathieu CE, Simon MC, Schumacker PT. Mitochondrial reactive oxygen species trigger hypoxia-induced transcription. Proc Natl Acad Sci U S A. 1998; 95:11715–11720. [PubMed: 9751731]
60. Kamata H, Honda S, Maeda S, Chang L, Hirata H, Karin M. Reactive oxygen species promote TNFalpha-induced death and sustained JNK activation by inhibiting MAP kinase phosphatases. Cell. 2005; 120:649–661. [PubMed: 15766528]
61. Finkel T. Signal transduction by reactive oxygen species. J Cell Biol. 2011; 194:7–15. [PubMed: 21746850]
62. Hamanaka RB, Chandel NS. Mitochondrial reactive oxygen species regulate cellular signaling and dictate biological outcomes. Trends Biochem Sci. 2010; 35:505–513. [PubMed: 20430626]

63. Bae YS, Kang SW, Seo MS, Baines IC, Tekle E, Chock PB, Rhee SG. Epidermal growth factor (EGF)-induced generation of hydrogen peroxide. Role in EGF receptor-mediated tyrosine phosphorylation. J Biol Chem. 1997; 272:217–221. [PubMed: 8995250]
64. Sundaresan M, Yu ZX, Ferrans VJ, Irani K, Finkel T. Requirement for generation of H2O2 for platelet-derived growth factor signal transduction. Science. 1995; 270:296–299. [PubMed: 7569979]
65. Woo HA, Yim SH, Shin DH, Kang D, Yu DY, Rhee SG. Inactivation of peroxiredoxin I by phosphorylation allows localized H(2)O(2) accumulation for cell signaling. Cell. 2010; 140:517–528. [PubMed: 20178744]
66. Salmeen A, Andersen JN, Myers MP, Meng TC, Hinks JA, Tonks NK, Barford D. Redox regulation of protein tyrosine phosphatase 1B involves a sulphenyl-amide intermediate. Nature. 2003; 423:769–773. [PubMed: 12802338]
67. Lee SR, Kwon KS, Kim SR, Rhee SG. Reversible inactivation of protein-tyrosine phosphatase 1B in A431 cells stimulated with epidermal growth factor. J Biol Chem. 1998; 273:15366–15372. [PubMed: 9624118]
68. Meng TC, Fukada T, Tonks NK. Reversible oxidation and inactivation of protein tyrosine phosphatases in vivo. Mol Cell. 2002; 9:387–399. [PubMed: 11864611]
69. Ishak KG, Zimmerman HJ, Ray MB. Alcoholic liver disease: pathologic, pathogenetic and clinical aspects. Alcohol Clin Exp Res. 1991; 15:45–66. [PubMed: 2059245]
70. Farrell GC, Larter CZ. Nonalcoholic fatty liver disease: from steatosis to cirrhosis. Hepatology. 2006; 43:S99–S112. [PubMed: 16447287]
71. Erickson SK. Nonalcoholic fatty liver disease. J Lipid Res. 2009; 50(Suppl):S412–416. [PubMed: 19074370]
72. Preiss D, Sattar N. Non-alcoholic fatty liver disease: an overview of prevalence, diagnosis, pathogenesis and treatment considerations. Clin Sci (Lond). 2008; 115:141–150. [PubMed: 18662168]
73. Sandler RS, Everhart JE, Donowitz M, Adams E, Cronin K, Goodman C, Gemmen E, Shah S, Avdic A, Rubin R. The burden of selected digestive diseases in the United States. Gastroenterology. 2002; 122:1500–1511. [PubMed: 11984534]
74. Younossi ZM, Stepanova M, Afendy M, Fang Y, Younossi Y, Mir H, Srishord M. Changes in the prevalence of the most common causes of chronic liver diseases in the United States from 1988 to 2008. Clin Gastroenterol Hepatol. 2011; 9:524–530. e521. quiz e560. [PubMed: 21440669]
75. Nagata K, Suzuki H, Sakaguchi S. Common pathogenic mechanism in development progression of liver injury caused by non-alcoholic or alcoholic steatohepatitis. J Toxicol Sci. 2007; 32:453–468. [PubMed: 18198478]
76. Lu Y, Cederbaum AI. CYP2E1 and oxidative liver injury by alcohol. Free Radic Biol Med. 2008; 44:723–738. [PubMed: 18078827]
77. Dey A, Cederbaum AI. Induction of cytochrome P450 2E1 [corrected] promotes liver injury in ob/ob mice. Hepatology. 2007; 45:1355–1365. [PubMed: 17538970]
78. Tilg H, Diehl AM. Cytokines in alcoholic and nonalcoholic steatohepatitis. N Engl J Med. 2000; 343:1467–1476. [PubMed: 11078773]
79. McNiven MA, Casey CA. Alcohol and lipid traffic don't mix. Hepatology. 2011; 53:1073–1075. [PubMed: 21384406]
80. Listenberger LL, Brown DA. Lipid droplets. Curr Biol. 2008; 18:R237–238. [PubMed: 18364222]
81. Guo Y, Cordes KR, Farese RV Jr. Walther TC. Lipid droplets at a glance. J Cell Sci. 2009; 122:749–752. [PubMed: 19261844]
82. Brasaemle DL, Wolins NE. Packaging of fat: an evolving model of lipid droplet assembly and expansion. J Biol Chem. 2012; 287:2273–2279. [PubMed: 22090029]
83. Murphy S, Martin S, Parton RG. Lipid droplet-organelle interactions; sharing the fats. Biochim Biophys Acta. 2009; 1791:441–447. [PubMed: 18708159]
84. Wang H, Sreenevasan U, Hu H, Saladino A, Polster BM, Lund LM, Gong DW, Stanley WC, Sztalryd C. Perilipin 5, a lipid droplet-associated protein, provides physical and metabolic linkage to mitochondria. J Lipid Res. 2011; 52:2159–2168. [PubMed: 21885430]

85. Robenek H, Hofnagel O, Buers I, Robenek MJ, Troyer D, Severs NJ. Adipophilin-enriched domains in the ER membrane are sites of lipid droplet biogenesis. J Cell Sci. 2006; 119:4215–4224. [PubMed: 16984971]

86. Lieber CS, DeCarli LM. Liquid diet technique of ethanol administration: 1989 update. Alcohol Alcohol. 1989; 24:197–211. [PubMed: 2667528]

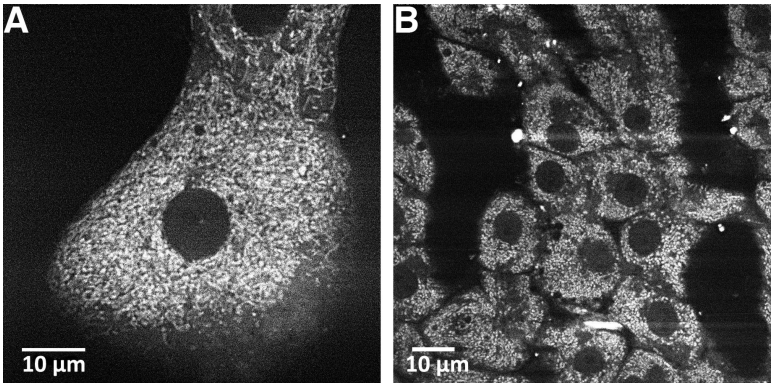

Fig. 1. Pyridine nucleotide fluorescence in hepatocytes

Confocal images depict NAD(P)H fluorescence in cultured hepatocytes (A) compared to hepatocytes in the intact perfused liver (B). Pyridine nucleotide fluorescence was detected with 720 nm multiphoton excitation as described in [38]. Images reproduced with permission [38].

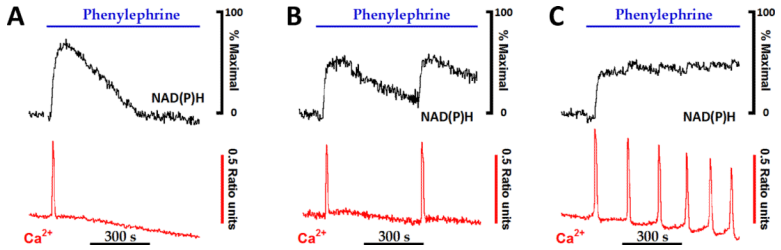

Fig. 2. The regulation of mitochondrial NAD(P)H production by increases in cytosolic calcium

Hepatocytes isolated from chow-fed rats were loaded with low levels of fura2/AM, as described previously [17, 18, 38], then stimulated with submaximal levels of phenylephrine, an α- adrenergic agonist. Agonist-evoked increases in fura-2 and NAD(P)H fluorescence intensities were monitored simultaneously [38]. NAD(P)H responses were normalized to the peak 360 nm fluorescence intensity changes obtained in the presence of rotenone plus ß-hydroxybutyrate (not shown). Data reproduced from [24] with permission.

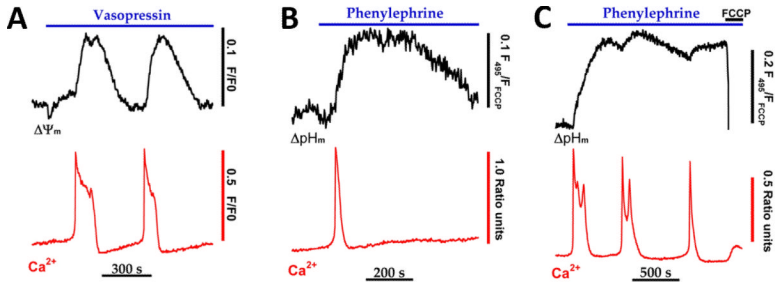

Fig. 3. Cytosolic calcium spikes stimulate a rise in mitochondrial proton motive force

Hepatocytes isolated from chow-fed rats were loaded with fura2/AM and TMREE (**A**) or fluorescein diacetate (**B-C**) then treated with submaximal hormone concentrations. Hormone-evoked increases in Ca^{2+} and mitochondrial membrane potential ($\Delta\Psi_m$) or Ca^{2+} and mitochondrial pH gradients (ΔpH_m) were monitored simultaneously as described [17, 38]. The protonophore, FCCP (5 μM), was added in **C** to completely collapse mitochondrial PMF. The data in panel A are reproduced from [38] with permission.

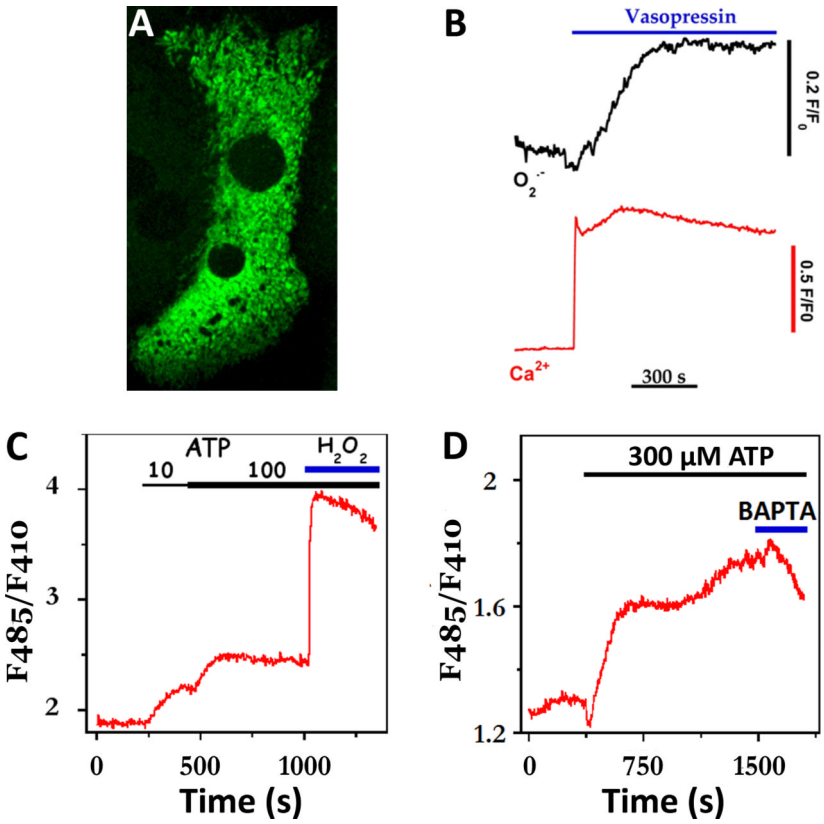

Fig. 4. Hormone-evoked increases in the rate of mitochondrial ROS formation

(**A**) Maximal intensity projection of two adjacent hepatocytes expressing mitochondrial-targeted cpYFP, a superoxide-sensitive fluorescent protein. (**B**) Simultaneous measurement of cytosolic Ca^{2+} and mitochondrial superoxide ($O_2^{\bullet-}$) increases evoked by maximal vasopressin concentrations (100 nM). Increases in Ca^{2+} were monitored with fura-2, while 485nm excitation of cpYFP was used to follow $O_2^{\bullet-}$ responses. Note: fura-2 overlaps with the 410nm portion of the cpYFP spectrum. (**C-D**) High levels of extracellular ATP evoke sustained increases in the production of mitochondrial H_2O_2. Production of H_2O_2 was monitored with mitochondrial targeted Hyper™ and alternating excitation at 485nm and 410nm. Exogenous H_2O_2 (100 µM) was added at the end of the run to maximally oxidize the biosensor (C). In panel D, excess BAPTA free acid (2 mM, blue bar) was added to chelate extracellular Ca^{2+}.

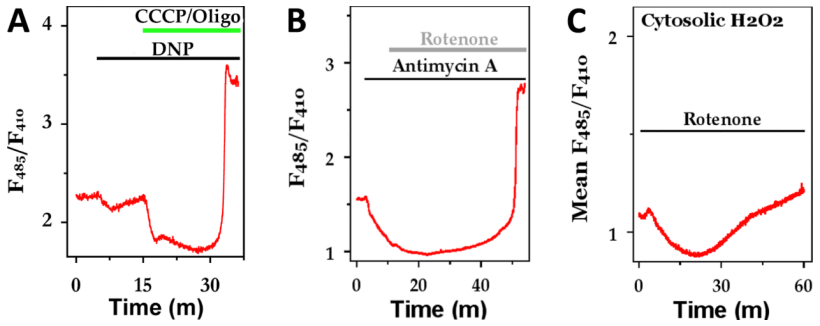

Fig 5. Reactive oxygen species formation in hepatocytes

(**A-B**) The effect of mitochondrial uncouplers and respiratory inhibitors on mitochondrial H_2O_2 production. (**C**) The effect of inhibiting mitochondrial respiration on cytosolic H_2O_2 production. Additions are dinitrophenol (DNP; 20μM), CCCP plus oligomycin (5 μM/ 1μg/ml), 1 μM antimycin A and 1 μM rotenone.

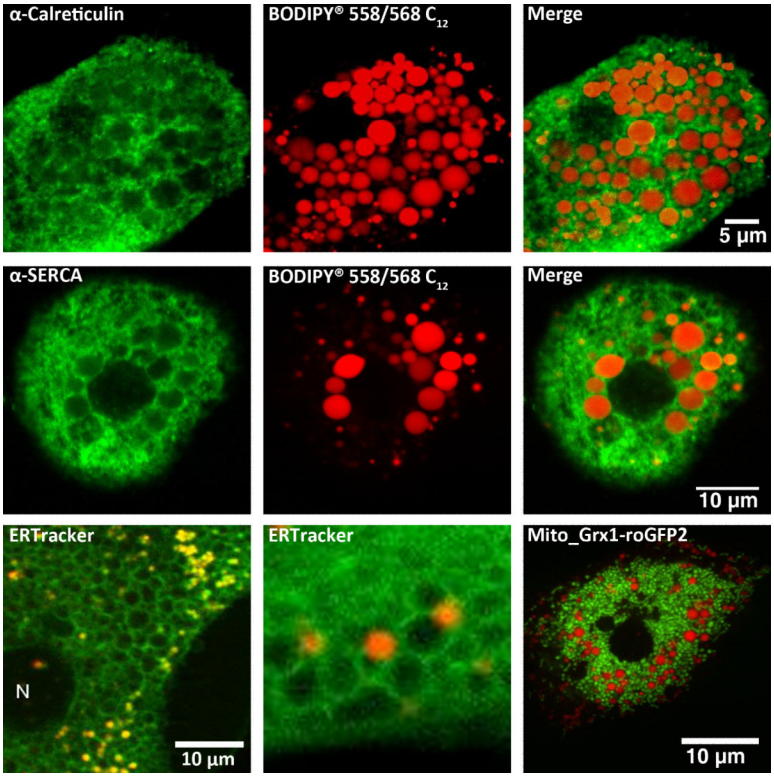

Fig 6. Lipid droplets

Hepatocytes isolated from alcohol-fed rats (top row) or their pair-fed littermate controls (middle row) were maintained in primary culture for 4 hrs. Lipid droplets were labeled for 2-4 hrs with the red fluorescent fatty acid analogue Bodipy® 558/568 C_{12} (red pseudocolor). Cells from pair-fed controls (middle row) were also incubated with 300 μM oleic acid to induce lipid droplet formation. Cultures were fixed with 1% paraformaldehyde and then immunoreactivity for calreticulin or SERCA (kind gift from Dr. J. Lytton) was determined. Top row: calreticulin immunoreactivity in an alcoholic hepatocyte. Middle row: SERCA immunoreactivity in a lipid-loaded control hepatocyte.

Bottom row: Live hepatocytes from chow-fed rats were stained with 200 nM ER tracker (green pseudocolor) and Bodipy® 558/568 C_{12} (red pseudocolor), or transfected with a mitochondrial targeted glutathione biosensor Grx1-roGFP2 (kind gift from Dr. T. Dick, green pseudocolor) then incubated with the fatty acid analogue (bottom right most panel).

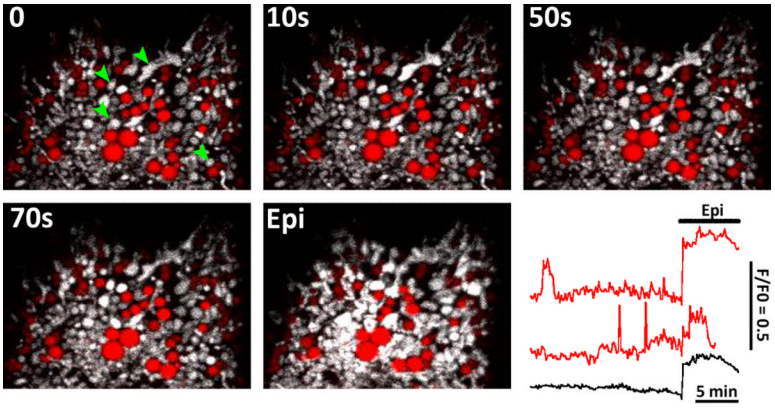

Fig 7. Spontaneous mitochondrial Ca^{2+} spikes and lipid droplets

Hepatocytes isolated from chow-fed rats were transfected with mitochondrial-targeted $GcamP_3$ (provided by Dr. L. Looger via Addgene) then incubated overnight with Bodipy® 558/568 C_{12} and oleic acid. Confocal images depict GcamP3 fluorescence intensity in gray scale and Bodipy® 558/568 C_{12} in red. Green arrowheads point to mitochondria that display spontaneous mitochondrial Ca^{2+} increases. The red traces show mitochondrial Ca^{2+} responses in single mitochondrion or mitochondrial clusters. The black trace is the whole cell calcium response. At the end of the run, the culture was treated with 1 μM epinephrine (Epi) to elicit a global cytosolic/mitochondrial calcium increase.